JACS
JOURNAL OF THE AMERICAN CHEMICAL SOCIETY

ARTICLE

pubs.acs.org/JACS

A 2D Covalent Organic Framework with 4.7-nm Pores and Insight into Its Interlayer Stacking

Eric L. Spitler,[†] Brian T. Koo,[‡] Jennifer L. Novotney,[†] John W. Colson,[†] Fernando J. Uribe-Romo,[†] Gregory D. Gutierrez,[†] Paulette Clancy,*[,‡] and William R. Dichtel*[,†]

[†]Department of Chemistry and Chemical Biology, Cornell University, Ithaca, New York 14853, United States

[‡]School of Chemical and Biomolecular Engineering, Cornell University, Ithaca, New York 14853, United States

Supporting Information

ABSTRACT: Two-dimensional layered covalent organic frameworks (2D COFs) organize π-electron systems into ordered structures ideal for exciton and charge transport and exhibit permanent porosity available for subsequent functionalization. A 2D COF with the largest pores reported to date was synthesized by condensing 2,3,6,7,10,11-hexahydroxytriphenylene (HHTP) and 4,4′-diphenylbutadiynebis(boronic acid) (DPB). The COF was prepared as both a high surface area microcrystalline powder as well as a vertically oriented thin film on a transparent single-layer graphene/fused silica substrate. Complementary molecular dynamics and density functional theory calculations provide insight into the interlayer spacing of the COF and suggest that adjacent layers are horizontally offset by 1.7−1.8 Å, in contrast to the eclipsed AA stacking typically proposed for these materials.

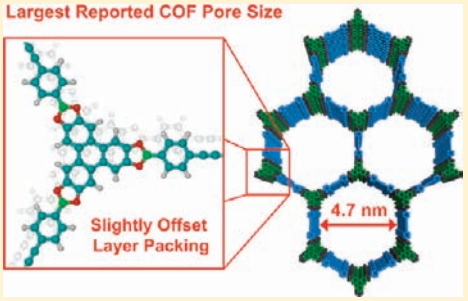

1. INTRODUCTION

Covalent organic frameworks (COFs) organize molecular building blocks into layered two-dimensional (2D)[1−10] or three-dimensional (3D)[11,12] periodic crystalline networks that feature high surface areas, excellent thermal stability, and extremely low densities. The layered 2D variants stack functional π-electron systems in van der Waals contact with maximal π-orbital overlap ideal for charge or exciton transport[5−7,13−15] and exhibit open porous channels that run parallel to the direction of stacking. These properties, in addition to the predictable nature of COF design, have attracted great interest as structurally precise optoelectronic materials. COFs are usually isolated as insoluble and unprocessable powders, but we recently reported the first oriented, crystalline COF films on transparent conductive substrates.[16] Oriented thin film morphologies broaden the potential applications of COFs significantly, as they might template the formation of other nanomaterials or enable nanometer-scale patterning;[17] however, these applications require pores larger than the typical 2−3 nm size range.[8,18] Here we describe a 2D COF (HHTP-DPB COF) with 4.7-nm wide hexagonal pores, the largest yet reported, which we synthesized as both an insoluble powder and as a vertically oriented thin film.

Nearly all 2D layered COFs have been described as fully eclipsed structures based on their powder X-ray diffraction (PXRD) patterns, but the relatively broad peaks do not rule out small horizontal offsets between layers.[19] We have performed a detailed molecular mechanics and density functional theory (DFT) modeling analysis of the interlayer potential energies of various stacking conformations of HHTP-DPB COF. These studies suggest that adjacent layers of HHTP-DPB COF are slightly offset (1.7−1.8 Å) from the true AA eclipsed packing structure previously proposed for these materials. Though these offsets are relatively small relative to the size of the COF unit cell, similar changes in packing dramatically affect the charge mobility of discotic liquid crystals.[20,21] Thus, our simulations are critical for optimizing future 2D layered COFs for efficient vertical charge transport.[22] Given the similarity of the HHTP-DPB COF to other 2D layered COF structures, we believe these offsets are likely to be found across the entire class of these materials.

2. RESULTS AND DISCUSSION

2.1. COF Powder Synthesis and Characterization. The solvothermal condensation of 4,4′-diphenylbutadiynebis(boronic acid) (**1**, DPB) with 2,3,6,7,10,11-hexahydroxytriphenylene (**2**, HHTP) in a 1:1 mixture of mesitylene:dioxane provided the HHTP-DPB COF as a microcrystalline powder (Scheme 1). **1** is an intriguing COF building block because of its linear structure, extended conjugation, and minimal steric conflicts associated with achieving a planar conformation. The HHTP-DPB COF powders were isolated from the reaction mixture by filtration and purified by washing with toluene and drying under vacuum. Fourier transform infrared spectroscopy (FTIR) indicated boronate ester formation, as evidenced by a sharp B−O stretch located at 1354 cm^{-1} not found in either of the reactants. The spectrum also showed strongly attenuated hydroxyl stretches. Spectra taken prior to activating the pores show intense $-CH_3$ stretches of

Received: July 12, 2011
Published: October 20, 2011

Scheme 1. Synthesis of HHTP-DPB COF from Bis(boronic acid) Linker 1 and HHTP 2 (left) and Model of the Idealized bnn Topology (right)

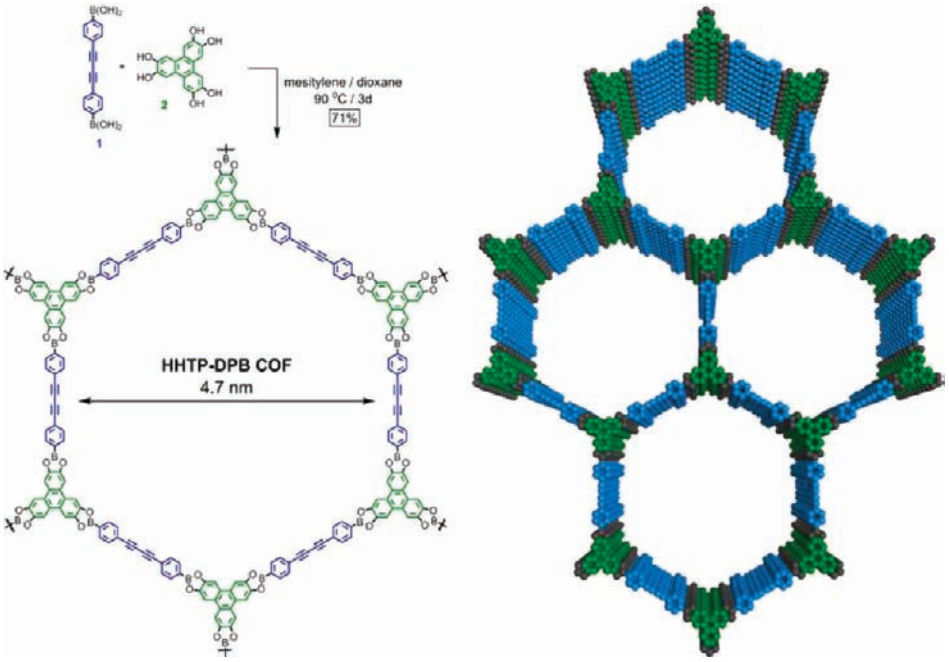

toluene or mesitylene, which disappear upon heating the COF at 90 °C under vacuum for 72 h. In contrast, we have successfully removed these solvents from other 2D layered COFs containing HHTP at room temperature under vacuum. $^{1}H-^{13}C$ CP/MAS NMR of HHTP-DPB COF confirmed the formation of the expected structure, and its ^{11}B NMR spectrum consisted of a single resonance consistent with the formation of a single type of boronate ester linkage (see Supporting Information).

The gas adsorption properties of HHTP-DPB COF were evaluated by N_2 gas adsorption at 77 K (Figure 1A). The material exhibits a reversible isotherm typical of mesoporous materials most resembling Type IV, in which gas adsorption by the pores occurs in two steps at $P/P_0 < 0.10$ and $0.20 < P/P_0 = 0.40$ pressures.[23] Analysis of the low-pressure region ($0.05 < P/P_0 < 0.20$) of the isotherm provides a Langmuir surface area of 1290 $m^2\ g^{-1}$ and BET surface area of 930 $m^2\ g^{-1}$ (see Figure S21, Supporting Information).[24] To compare the measured gas adsorption capacity of the prepared COF with its maximum uptakes, we simulated an isotherm using Monte Carlo simulations using the Metropolis method in Materials Studio (Figure S22, Supporting Information), from which a maximum BET surface area of 2640 $m^2\ g^{-1}$ was calculated. This value is quite similar to the calculated Connolly surface area of 2670 $m^2\ g^{-1}$ for the eclipsed HHTP-DPB COF structure and consistent with that observed in other frameworks. These calculations suggest that the measured COF has been activated to approximately 40% of its maximum uptake, and further optimization is ongoing. The hysteresis observed during desorption is typical of interparticle adsorption and has been observed in other COFs. These particles were uniform spheres with 4 μm diameters, as observed by scanning electron microscopy (SEM, Figure 1B). HHTP-DPB COF retained 92% of its mass up to 350 °C by thermal gravimetric analysis (Figure S20, Supporting Information).

The crystallinity and unit cell parameters of the HHTP-DPB COF were determined by PXRD (Cu Kα line, Figure 2). The PXRD patterns of HHTP-DPB COF showed poor crystallinity prior to activation (Figure S15, Supporting Information), which improved dramatically after activating the COF under vacuum at 100 °C for 12 h. The diffraction pattern of the activated material shows peaks at 2.17°, 3.79°, 5.90°, 7.93°, and 8.02°, which correspond to the (100), (110), (210), (220), and (310) Bragg peaks of a primitive hexagonal lattice. The crystal structure was simulated using the Materials Studio suite of programs[25] by assembling eclipsed triphenylenes into a bnn net (*P6/mmm*).[26] The experimental PXRD displayed a diffraction pattern in agreement with one simulated from this model, allowing facile indexing of the diffraction peaks. Pawley refinement (Figure S18, Supporting Information) of the pattern gave unit cell parameters $a = b = 46.9$ Å. The broad (001) diffraction peak at 25.8° corresponds to a vertical spacing between stacked sheets of 3.37 Å, indicating that adjacent layers are in van der Waals contact. The relative positions of the butadiyne groups in the COF lattice lack the appropriate spacing and angular offset necessary to undergo topochemical polymerization,[27−29] and we saw no evidence for this process by differential scanning calorimetry or by heating the COF powders. We also considered an alternate structure wherein adjacent sheets are not cofacially stacked but offset by half of the unit cell distance in the horizontal *a* and *b* planes, thus creating a gra net ($P6_3/mmc$; Figure S19, Supporting Information). The simulated PXRD pattern of these structures did not match the experimental data.

2.2. Simulation of HHTP-DPB COF Interlayer Packing. It is important to note that almost all other 2D COFs have been described as eclipsed layered structures, but the X-ray diffraction peaks of these materials are too broad to preclude slight interlayer offsets. We performed complementary simulations to understand the 2D stacking of HHTP-DPB COF beyond the information available from the PXRD data. Two levels of theory were used to model the intermolecular interactions between COF layers:

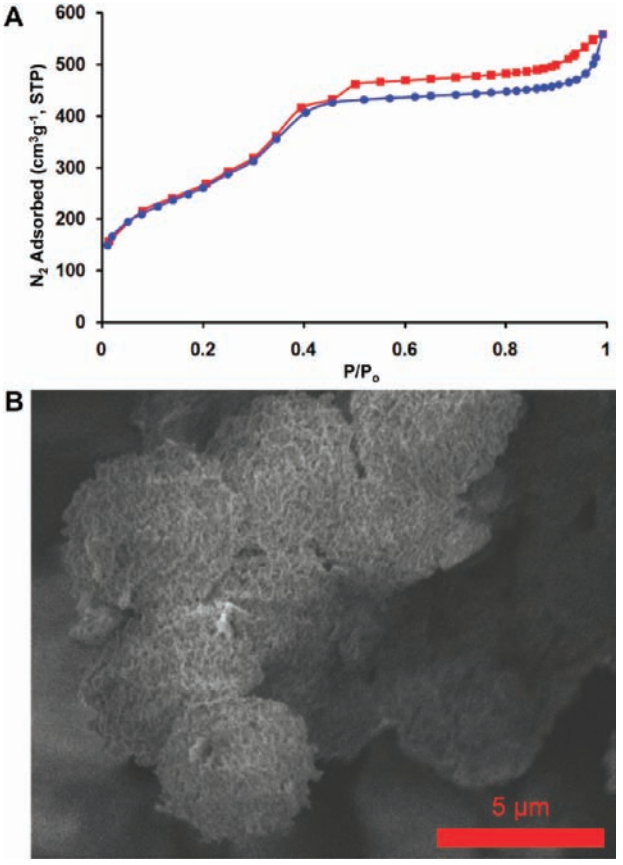

Figure 1. (A) N_2 adsorption (blue circles) and desorption (red squares) isotherms for HHTP-DPB COF. (B) Scanning electron microscope (SEM) image of HHTP-DPB COF powder.

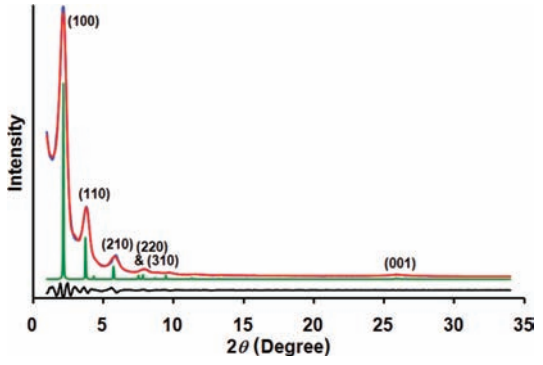

Figure 2. Experimental (blue) and Pawley refined (red) vs predicted (green) PXRD patterns of HHTP-DPB COF and difference plot (experimental, refined; black). Major observed reflections are labeled.

molecular mechanics, using the MM3 force field, which describes hydrocarbon and ringed aromatic systems reliably,[30,31] and DFT, a more accurate quantum mechanical treatment that accounts for electronic interactions.[32] Molecular dynamics simulations are orders of magnitude faster than static DFT calculations and can explore a far broader set of configurations. Therefore, we used molecular mechanics to broadly define the potential energy surface (PES) associated with offsetting two layers of the HHTP-DPB COF and subsequently refined this model in regions of interest using DFT.

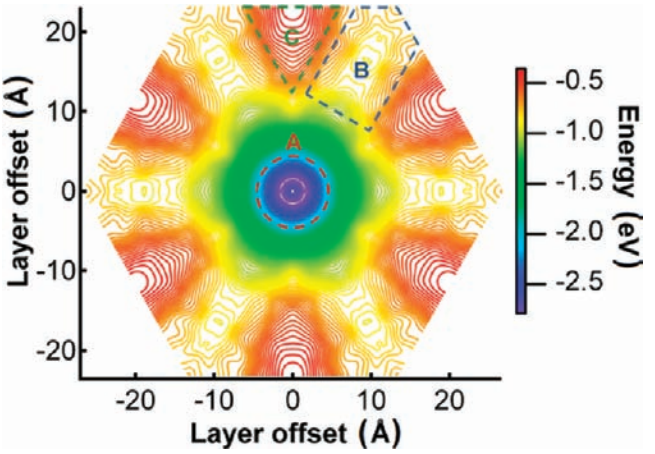

Figure 3. Potential energy surface generated from the semiempirical MM3 potential. The surface can be divided into three regions with distinct energetic properties: A, Low energy region containing eclipsed and near-eclipsed two-layer structures; B, region containing all staggered structures, shown schematically in Figure 4A; C, high-energy region containing the structures shown in Figure 4B.

The MM3-derived PES (Figure 3) was generated by varying the *x*- and *y*-translational offsets of two adjacent COF layers and recalculating the interlayer spacing at each point to minimize the interaction energy. The PES contains three regions (labeled A−C) of relatively flat 'terrain' bounded by steep gradients. Region A exhibits significantly more stabilizing interaction energies (−2.8 eV) than regions B and C (−0.8 and −0.4 eV, respectively) and corresponds to structures that are eclipsed or nearly eclipsed. The interlayer spacing that minimizes the interaction energy in this region is 3.45 Å, which is within 0.1 Å of the experimental value. In the MM3 calculations, the potential energy of the fully eclipsed structure is only 0.13 eV higher than the minimum energy calculated in region A, which occurs at offsets that define a ring of radius 1.6 Å around the origin. This result indicates almost no preference for nearly eclipsed structures, but repulsive electrostatic forces that occur at the origin are likely to be underestimated at the MM3 level of theory.

Regions B and C of the PES correspond to offsets that reduce the van der Waals contact between layers, each of which is higher in energy than region A. The flatter regions at the corners of the PES form region B, which correspond to gra layers (see Figure 4B). The potential energy in this region varies from a peak of about −0.7 eV to a valley of about −0.9 eV. The average binding energy of this region is less than a third of the binding energy of near-eclipsed structures in region A. The energy difference between regions A and B is about 2.0 eV, which is a very significant potential energy increase from the bottom of the potential energy well in region A. There are no significant potential energy barriers that might prevent reorganization of COF layers from region B to region A, suggesting that forming these structures is unlikely. As shown in Figure 4, there is less overlap in this configuration than in a more eclipsed configuration, which lowers the contribution of the van der Waals component to the intermolecular energy. However, monopoles in adjacent layers are staggered by 60° so that the repulsive interaction between them is less than in the eclipsed case. The potential energy gradient near staggered configurations is less steep than the gradient near eclipsed configurations because near-staggered configurations balance the decrease in HHTP overlap with an increase in linker overlap. Configurations

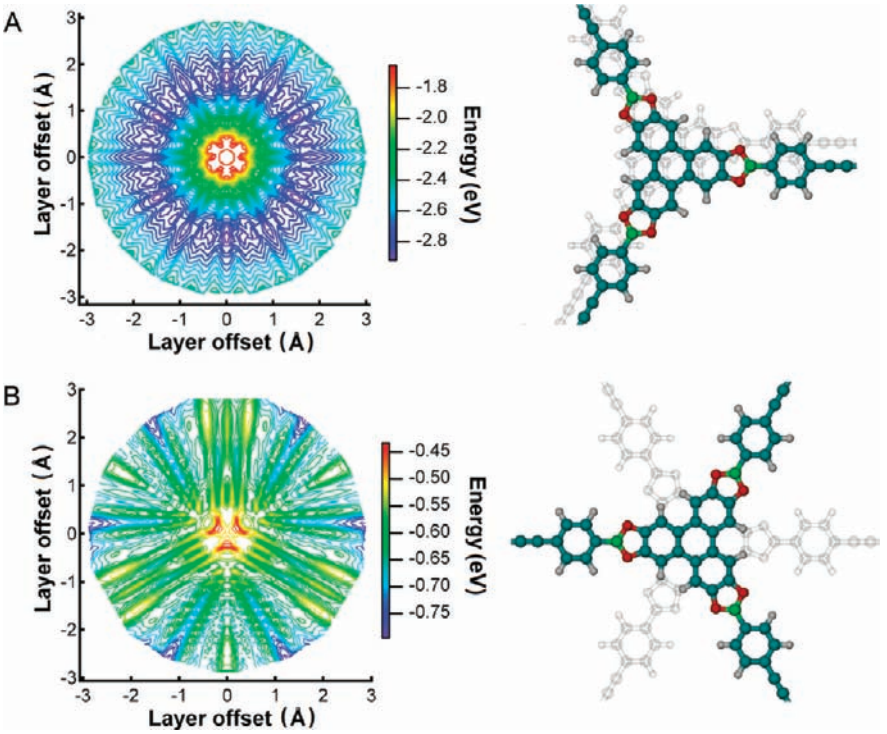

Figure 4. (A) Expansion of region A in Figure 3 calculated with density functional theory. (B) Expansion of a subset of region B in Figure 3 calculated with density functional theory and atomic representation of the two-layer staggered structure.

of layers with the highest potential energy are the triangle-shaped protrusions near the edges of the PES, labeled as region C in Figure 3. The energy of arrangements in this region is approximately −0.4 eV, which is 0.4 eV higher than the energies in region B, and 2.4 eV higher than arrangements in region A. The gradient between regions B and C attains a maximum value of 0.1 eV/Å. Because there is a constant negative gradient in region C, these structures are also unstable and unlikely to form. These are the most energetically unfavorable configurations because the structures have no molecular overlap between HHTP units and only minimal overlap of linkers in adjacent layers. This reduces the van der Waals component of the intermolecular energy to the smallest value possible and significantly raises the potential energy of structures in this region. On the basis of these findings, we did not perform further calculations on structures in region C

We next generated a new PES (Figure 4) for regions A and B using more accurate DFT calculations as expressed in Gaussian09 using the M06 exchange correlation functional.[32−34] The overall potential energy surface is qualitatively similar to that generated from the MM3 potential but with more finely corrugated surface features. Configurations with the lowest energy, of about −2.9 eV, are found 1.7−1.8 Å from the origin with an interlayer spacing of 3.42 Å, which is close to the experimental value and matches that of other 2D COFs. DFT calculations for structures in region B confirm that staggered structures remain significantly higher in energy (2.4 eV) than the eclipsed structures of region A. Thus, the MM3 model can give a reasonably accurate result for COF structures in a fraction of the time needed for ab initio calculations.

Despite the qualitative agreement between the MM3 and DFT calculations, there are important differences between the two approaches. The DFT PES suggests that fully eclipsed structures are unlikely, because they show a potential energy maximum −1.8 eV, significantly higher (1.1 eV) than that for the more stable structures just 1.7−1.8 Å away. These differences arise from DFT's more precise treatment of electrostatic forces. The variation in potential energy around the ring is 0.1 eV, compared with the insignificant 3×10^{-3} eV variations predicted by MM3. The net result is that, while MM3-generated results suggest that perfectly eclipsed structures are accessible, DFT calculations predict this is much less likely. Because this offset has no preferred direction, the average representation of the 3D structure of the COF cannot be reduced to a simple monoclinic unit cell. It is unlikely that there will be a prevalence of patterns, such as staircase, zigzag, or helical arrangements of layers that would be observable by X-ray diffraction. Instead, adjacent layers are more likely to stack in random arrangements around a preferred offset from the origin, similar to turbostratic disorder commonly observed in layered materials. These random offsets are difficult to observe in low resolution powder diffraction data, as they would generally affect only the relative intensity and width of certain diffraction peaks, while affecting peak positions only at small *d*-spacings (neither of which has been observed experimentally). We also compared the accessible surface area from the Connolly surfaces for eclipsed HHTP-DPB COF with that for 1.0 Å and 1.7 Å interlayer offsets. No significant differences were found, as each of these structures had accessible surface areas close to 2700 $m^2 g^{-1}$ (Table S2, Supporting Information). Thus, most methods used for COF characterization are unable to distinguish between eclipsed and slightly offset structures. In COFs designed for optoelectronic applications, small changes in these offsets will strongly affect charge mobilities through the stacked aromatic systems,[21] and the computational methods described above will be important to understand their performance and design optimal new materials.

2.3. Synthesis and Characterization of Vertically Oriented HHTP-DPB COF Films on Single Layer Graphene. Despite

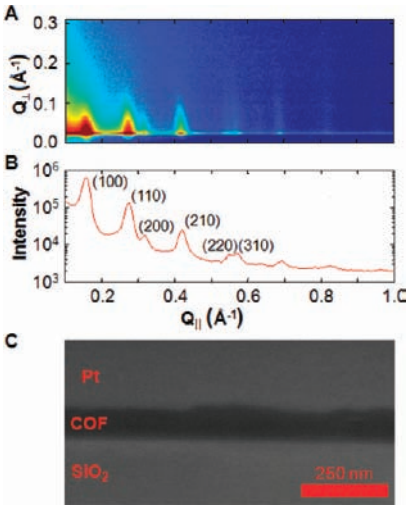

Figure 5. (A) Grazing incidence X-ray diffraction (GID) of HHTP-DPB COF thin film on SLG (growth time: 24 h). (B) Projection of A near $Q_{\perp} = 0$. (C) Cross-sectional SEM image of the film.

their intriguing structures, it remains difficult to perform advanced spectroscopy on COF powders or incorporate them into devices. We overcame this limitation recently by growing COF thin films on single-layer graphene (SLG) functionalized substrates.[16] We prepared crystalline, vertically oriented HHTP-DPB COF thin films by condensing **1** and **2** under solvothermal conditions in the presence of SLG on a transparent fused SiO_2 substrate (SLG/SiO_2). Grazing incidence X-ray diffraction (GID, Figure 5A) indicates scattering intensity at 0.156 $Å^{-1}$, 0.271 $Å^{-1}$, 0.311 $Å^{-1}$, 0.411 $Å^{-1}$, 0.543 $Å^{-1}$, and 0.568 $Å^{-1}$, corresponding to the same (100), (110), (200), (210), (220), and (310) peaks observed in the powder samples. The intensity of these diffractions is concentrated near $Q_{\perp} = 0$, indicating that the *c*-axis of the COF is oriented normal to the substrate surface. The (001) Bragg peak that appears at $Q_{\parallel} = 1.83$ $Å^{-1}$ in powder samples is not observed in the GID experiment (Figure S25, Supporting Information), again indicating that the *c*-axis is specifically oriented normal to the substrate. Instead, the (001) peak is observed at $Q_{\perp} = 1.85$ $Å^{-1}$ in measurements performed at large out-of-plane diffraction angles (Figure S26, Supporting Information). Top-down SEM images indicate that the films are featureless over large areas and have only occasional bulk crystallites distributed across the surface (Figure S27, Supporting Information). Cross-sectional micrographs obtained by milling the sample using a Ga^{+} focused ion beam indicate that the films are continuous across the substrate with thickness 132 ± 18 nm (Figure 5C). The large pore size obtained in the thin film morphology may also serve as a useful template for nanopatterning, as features in the 2−5 nm region are difficult to obtain using either standard lithographic techniques or block copolymer lithography.[35]

The HHTP-DPB COF powders and films are strongly photoluminescent (Figure 6), which we attribute to the cofacially packed diphenylbutadiyne subunits, as other HHTP-containing COFs do not fluoresce strongly. UV/vis spectra of the films obtained through the transparent SLG/SiO_2 substrate are consistent with the presence of the triphenylene and diphenylbutadiyne chromophores and show only moderate tailing at longer wavelengths associated with scattering. Photoemission spectra of the films show a λ_{max} of 457 nm (λ_{exc} = 357 nm) that is red-shifted by 55 nm relative to that of **1** dissolved in DMF. Several

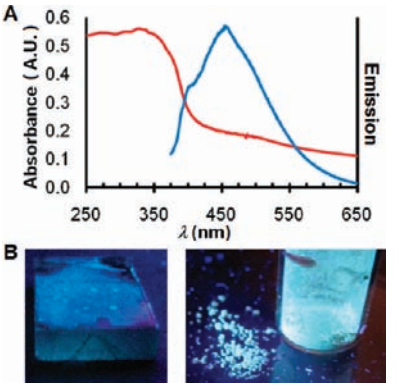

Figure 6. (A) Transmission absorption (red) and normalized emission (blue) spectra of HHTP-DPB COF thin film (λ_{exc} = 357 nm) and (B) photographs of fluorescent COF film on SLG/SiO_2 (left) and powder (right) under 365 nm illumination.

aspects of the COF structure impact the fluorescence of the diphenylbutadiyne chromophores. First, catechol boronate ester linkages have shown evidence of extended conjugation in linear polymers.[36] Though the conjugation efficiency of these groups is not as high as other linkages, this effect should be maximized in a COF given the coplanar relationship among the chromophores. Similarly, diphenylbutadiynes capable of free rotation of each phenyl group generally have very low fluorescence quantum yields, which increase dramatically when the phenyl rings are fixed into a coplanar arrangement.[37,38] Finally, vertical stacking of the diphenylbutadiynes can also lead to a red-shifted emission.[39−41]

3. CONCLUSIONS

We have demonstrated that the pore sizes of oriented 2D layered COF films can be pushed well into the mesoporous regime, which significantly expands the range of complementary molecular, polymeric, or inorganic guests that might be co-organized with these unique materials. Our computational studies strongly suggest that 2D layered COFs do not adopt true eclipsed structures usually reported for these materials, but that the layers are slightly offset from one another. These calculations are easily generalized to other 2D layered COFs and will be critical for understanding interlayer exciton and charge transport, two processes of fundamental importance for COF-based optoelectronic devices. Highly luminescent COF films are of interest for fluorescent sensors,[42,43] for which structural precision, tunable composition, and high surface areas will prove extremely useful.

■ ASSOCIATED CONTENT

Supporting Information. Experimental procedures and characterization data for all new compounds and materials and more details on the offset calculations and simulated surface area of HHTP-DPB COF. This material is available free of charge via the Internet at http://pubs.acs.org.

■ AUTHOR INFORMATION

Corresponding Author
wdichtel@cornell.edu; pc@cbe.cornell.edu

■ ACKNOWLEDGMENT

W.R.D. acknowledges support from the NSF CAREER program (CHE-1056657) and the NSF-funded CCI-I Center for Molecular Interfacing (CHE-0847926). This work is based upon research conducted at the Cornell High Energy Synchrotron Source (CHESS), which is supported by the National Science Foundation and the National Institutes of Health/National Institute of General Medical Sciences under NSF award DMR-0936384. We also made use of the Cornell Center for Materials Research (CCMR) facilities with support from the NSF Materials Research Science and Engineering Centers (MRSEC) program (DMR-0520404). E.L.S. acknowledges the award of the American Competitiveness in Chemistry postdoctoral fellowship (ACC-F) from the NSF (CHE-0936988). B.T.K. acknowledges the NSF Integrative Graduate Education and Research Traineeship (IGERT) Program in Materials for a Sustainable Future (DGE-0903653). J.L.N. acknowledges the NSF IGERT Program in the Nanoscale Control of Surfaces and Interfaces (DGE-0654193). J.W.C. acknowledges the award of a Graduate Research Fellowship from the NSF. We thank Dr. Arthur Woll at CHESS for helpful discussions.

■ REFERENCES

(1) Côté, A. P.; Benin, A. I.; Ockwig, N. W.; O'Keeffe, M.; Matzger, A. J.; Yaghi, O. M. *Science* **2005**, *310*, 1166–1170.
(2) Tilford, R. W.; Gemmill, W. R.; zur Loye, H. C.; Lavigne, J. J. *Chem. Mater.* **2006**, *18*, 5296–5301.
(3) Côté, A. P.; El-Kaderi, H. M.; Furukawa, H.; Hunt, J. R.; Yaghi, O. M. *J. Am. Chem. Soc.* **2007**, *129*, 12914–12915.
(4) Tilford, R. W.; Mugavero, S. J.; Pellechia, P. J.; Lavigne, J. J. *Adv. Mater.* **2008**, *20*, 2741–2746.
(5) Wan, S.; Guo, J.; Kim, J.; Ihee, H.; Jiang, D. *Angew. Chem., Int. Ed.* **2008**, *47*, 8826–8830.
(6) Wan, S.; Guo, J.; Kim, J.; Ihee, H.; Jiang, D. *Angew. Chem., Int. Ed.* **2009**, *48*, 5439–5442.
(7) Spitler, E. L.; Dichtel, W. R. *Nat. Chem.* **2010**, *2*, 672–677.
(8) Dogru, M.; Sonnauer, A.; Gavryushin, A.; Knochel, P.; Bein, T. *Chem. Commun.* **2011**, *47*, 1707–1709.
(9) Spitler, E. L.; Giovino, M. R.; White, S. L.; Dichtel, W. R. *Chem. Sci.* **2011**, *2*, 1588–1593.
(10) Feng, X.; Chen, L.; Dong, Y.; Jiang, D. *Chem. Commun.* **2011**, *47*, 1979–1981.
(11) El-Kaderi, H. M.; Hunt, J. R.; Mendoza-Cortes, J. L.; Cote, A. P.; Taylor, R. E.; O'Keeffe, M.; Yaghi, O. M. *Science* **2007**, *316*, 268–272.
(12) Uribe-Romo, F. J.; Hunt, J. R.; Furukawa, H.; Klöck, C.; O'Keeffe, M.; Yaghi, O. M. *J. Am. Chem. Soc.* **2009**, *131*, 4570–4571.
(13) Ding, X.; Guo, J.; Feng, X.; Honsho, Y.; Guo, J.; Seki, S.; Maitarad, P.; Saeki, A.; Nagase, S.; Jiang, D. *Angew. Chem., Int. Ed.* **2011**, *50*, 1289–1293.
(14) Ding, X.; Chen, L.; Honsho, Y.; Feng, X.; Saengsawang, O.; Guo, J.; Saeki, A.; Seki, S.; Irle, S.; Nagase, S.; Parasuk, V.; Jiang, D. *J. Am. Chem. Soc.* **2011**, *133*, 14510–14513.
(15) Wan, S.; Gándra, F.; Asano, A.; Furukawa, H.; Saeki, A.; Dey, S. K.; Liao, L.; Ambrogio, M. W.; Botros, Y. Y.; Duan, X. F.; Seki, S.; Stoddart, J. F.; Yaghi, O. M. *Chem. Mater.* **2011**, *23*, 4094–4097.
(16) Colson, J. W.; Woll, A. R.; Mukherjee, A.; Levendorf, M. P.; Spitler, E. L.; Shields, V. B.; Spencer, M. G.; Park, J.; Dichtel, W. R. *Science* **2011**, *332*, 228–231.
(17) Berlanga, I.; Ruiz-González, M. L.; González-Calbet, J. M.; Fierro, J. L. G.; Mas-Ballesté, R.; Zamora, F. *Small* **2011**, *7*, 1207–1211.
(18) Dogru, M.; Bein, T. *Nat. Nanotechnol.* **2011**, *6*, 333–335.
(19) Lukose, B.; Kuc, A.; Heine, T. *Chem.—Eur. J.* **2011**, *17*, 2388–2392.
(20) Cornil, J.; Lemaur, V.; Calbert, J. P.; Brédas, J. L. *Adv. Mater.* **2002**, *14*, 726–729.
(21) Coropceanu, V.; Cornil, J.; da Silva Filho, D. A.; Olivier, Y.; Silbey, R.; Brédas, J.-L. *Chem. Rev.* **2007**, *107*, 926–952.
(22) Patwardhan, S.; Kocherzhenko, A. A.; Grozema, F. C.; Siebbeles, L. D. A. *J. Phys. Chem. C* **2011**, *115*, 11768–11772.
(23) Sing, K. S. W.; Everett, D. H.; Haul, R. A. W.; Moscou, L.; Pierotti, R. A.; Rouquerol, J.; Siemieniewska, T. *Pure Appl. Chem.* **1985**, *57*, 603–619.
(24) Walton, K. S.; Snurr, R. Q. *J. Am. Chem. Soc.* **2007**, *129*, 8552–8556.
(25) *Accelrys*, 4.4 ed.; Accelrys Software, San Diego, 2008.
(26) O'Keeffe, M.; Peskov, M. A.; Ramsden, S. J.; Yaghi, O. M. *Acc. Chem. Res.* **2008**, *41*, 1782–1789.
(27) Coates, G. W.; Dunn, A. R.; Henling, L. M.; Dougherty, D. A.; Grubbs, R. H. *Angew. Chem., Int. Ed.* **1997**, *36*, 248–251.
(28) Li, Z.; Fowler, F. W.; Lauher, J. W. *J. Am. Chem. Soc.* **2009**, *131*, 634–643.
(29) Deschamps, J.; Balog, M.; Boury, B.; Ben Yahia, M.; Filhol, J.-S.; van der Lee, A.; Al Choueiry, A.; Barisien, T.; Legrand, L.; Schott, M.; Dutremez, S. G. *Chem. Mater.* **2010**, *22*, 3961–3982.
(30) Allinger, N. L.; Yuh, Y. H.; Lii, J. H. *J. Am. Chem. Soc.* **1989**, *111*, 8551–8566.
(31) Cantrell, R.; Clancy, P. *Surf. Sci.* **2008**, *602*, 3499–3505.
(32) Jacquemin, D.; Perpéte, E. A.; Ciofini, I.; Adamo, C.; Valero, R.; Zhao, Y.; Truhlar, D. G. *J. Chem. Theory Comput.* **2010**, *6*, 2071–2085.
(33) Zhao, Y.; Truhlar, D. G. *Theor. Chem. Acc.* **2008**, *120*, 215–241.
(34) Zhao, Y.; Truhlar, D. G. *J. Chem. Phys.* **2009**, *130*, 074103.
(35) Tang, C.; Lennon, E. M.; Fredrickson, G. H.; Kramer, E. J.; Hawker, C. J. *Science* **2008**, *322*, 429–432.
(36) Niu, W.; Smith, M. D.; Lavigne, J. J. *J. Am. Chem. Soc.* **2006**, *128*, 16466–16467.
(37) Mizobe, Y.; Ito, H.; Hisaki, I.; Miyata, M.; Hasegawa, Y.; Tohnai, N. *Chem. Commun.* **2006**, 2126–2128.
(38) Shanks, D.; Preus, S.; Qvortrup, K.; Hassenkam, T.; Nielsen, M. B.; Kilsa, K. *New J. Chem.* **2009**, *33*, 507–516.
(39) Egbe, D. A. M.; Ulbricht, C.; Orgis, T.; Carbonnier, B.; Kietzke, T.; Peip, M.; Metzner, M.; Gericke, M.; Birckner, E.; Pakula, T.; Neher, D.; Grummt, U.-W. *Chem. Mater.* **2005**, *17*, 6022–6032.
(40) Egbe, D. A. M.; Birckner, E.; Klemm, E. *J. Polym. Sci., Part A: Polym. Chem.* **2002**, *40*, 2670–2679.
(41) Goichi, M.; Miyahara, H.; Toyota, S. *Chem. Lett.* **2006**, *35*, 920–921.
(42) Thomas, S. W.; Joly, G. D.; Swager, T. M. *Chem. Rev.* **2007**, *107*, 1339–1386.
(43) Allendorf, M. D.; Bauer, C. A.; Bhakta, R. K.; Houk, R. J. T. *Chem. Soc. Rev.* **2009**, *38*, 1330–1352.